Journal of Materials Chemistry A

PAPER

View Article Online
View Journal | View Issue

Cite this: J. Mater. Chem. A, 2014, 2, 7471

Graphene enhanced carbon-coated tin dioxide nanoparticles for lithium-ion secondary batteries†

Zhongtao Li,‡ Guiliang Wu,‡ Dong Liu, Wenting Wu, Bo Jiang, Jingtang Zheng, Yanpeng Li, Junhua Li and Mingbo Wu*

Received 21st January 2014
Accepted 5th March 2014

DOI: 10.1039/c4ta00361f

www.rsc.org/MaterialsA

A one-step, scalable method has been developed to prepare SnO_2 based carbon materials. Their performances as anodes for lithium-ion batteries can be improved through simultaneous growth of SnO_2 nanoparticles, a carbonaceous polymer coating and "doping" of graphene oxide (GO) by thermal treatment. Detailed characterization of the resulting composite materials using transmission electron microscopy and X-ray diffraction suggests that "doping" a certain amount of GO could clearly change the crystallinity and distribution of SnO_2 nanoparticles in the mixture. The SnO_2 based carbon material exhibits a stable reversible capacity of 720 mA h g^{-1} after 70 cycles as the anode of lithium-ion batteries, indicating that the composites might have a promising future application in Li-ion batteries.

1. Introduction

Lithium-ion secondary batteries (LIBs) play an essential role in electronic devices in the modern world, such as in communication devices, portable devices, and electrical/hybrid vehicles. Even though LIBs have many advantages like high electromotive force and high energy density, the requirements on their specific capability, charging stability and rate capability are increasing with the development of technology. Many research attempts have been made to explore new electrode materials or design novel nanostructures of electrode materials to meet the new demands.[1–3] For an anode material in LIBs, graphite is usually employed as a standard electrode because it can be reversibly charged and discharged under intercalation potentials with reasonable specific capacity.[4] To increase the battery's capability, some elements or compounds (*e.g.* Sn, Sb, Si or Ge) alloyed to lithium with much larger specific capacities than commercial graphite are adopted to replace the carbon-based anode.[5–8]

Among these studies, the electrochemical reactivity of SnO_2 has drawn much attention, due to its high theoretical capacity (782 mA h g^{-1}) during the cyclic process.[9,10] And, the tin dioxide anode has a higher operating voltage than graphite, so the safety of batteries during the rapid charge–discharge cycle could be improved.[11] However, the practical uses of the tin oxide materials are restricted, because they suffer a severe volume variation (around 300%) during Li^+ insertion and extraction. This effect often causes electrode disintegration and rapid capacity fading.[12] To solve these problems, various nanostructured SnO_2 and SnO_2 composites have been proposed with the aim of stabilizing the active electrode material by accommodating the volume change during the cyclic process.[13,14] Metal oxide particles with small size and homogeneous carbon coating have already been reported to improve the mechanical stability and the electrochemical performances because of the buffering effect and low activity of the carbon coating.[15,16] An electrochemical improvement in the performances of the SnO_2/carbon nanocomposites is achieved due to the role of the carbon support which enables a better accommodation of the large volume change and improves the electron conductivity of the electrode.[17]

As has been reported previously glucose, sucrose and some other water soluble polysaccharides as the widely used precursors were carbonized by thermal treatment to form a carbon matrix for tolerating the SnO_2 nanocrystal.[9,18] However, the capacity retention of some of the reported carbon-coated materials is still limited, which mainly arises from the relative inhomogeneous nanoparticles and the low conductivity of coated carbon.[19,20] Moreover, some of the previous methods for producing carbon-coated materials were relatively complicated and the core–shell nanostructure was usually obtained in a multistep approach.[21,22] Thus it has remained a challenge to find an approach that can simultaneously ensure both the homogeneous dispersion of SnO_2 nanoparticles (NPs) and the construction of a conductive carbon matrix.

Graphene (GN) also has recently been investigated as the functional matrix support for SnO_2-based nanostructures due to its intrinsic properties such as flexible two-dimensional structure, high surface area (over 2600 m^2 g^{-1}) and excellent electrical conductivity, which not only facilitate the transfer of electrons and the transport of the electrolyte in the electrode,

State Key Laboratory of Heavy Oil Processing, China University of Petroleum, Qingdao 266580, China. E-mail: wumb@upc.edu.cn; Tel: +86 532 8698 3452

† Electronic supplementary information (ESI) available. See DOI: 10.1039/c4ta00361f

‡ These authors contributed equally to this work.

but also diminish the stress of the collective electrode upon battery cycling.[23,24] However, the SnO_2-based nanoparticles could be easily peeled off from the graphene and afterwards pass through the pores of the separator, and finally agglomerate on the anode, leading to self-discharge, capacity loss and even electrode failure.[25] Meanwhile, for the cost control of practical application, the content of more expensive GN in the materials should be kept at a reasonable level. Therefore, it is greatly important to develop a facile and reliable approach to synthesize desirable nanocomposites that can reliably bind SnO_2-based nanostructures with graphene to avoid such issues.

In order to overcome these problems, many kinds of SnO_2/carbon composites for LIBs have been reported, most of which adopted a great amount of GN to form the supporting matrix or multistep approaches.[26–28] Few reports on the SnO_2/C/GN composite have been published: Liang and co-workers reported a SnO_2–polyaniline–reduced graphene oxide anode in LIBs which presents a discharge capacity of 574 mA h g^{-1} after 50 cycles, which corresponds to 74% of its theoretical specific capacity.[29] Li and co-workers reported a SnO_2–carbon–RGO composite with a specific discharge capacity of 862 mA h g^{-1} in the initial cycle and a discharge capacity of 622 mA h g^{-1} after 100 cycles.[30] Zhang and co-workers reported carbon-coated SnO_2/graphene nanosheets, which present an initial capacity of 1310 mA h g^{-1} and 757 mA h g^{-1} can be retained after 150 cycles, which contain 10 wt% graphene in the composite.[31]

Herein, we have attempted to prepare homogeneous carbon coated SnO_2 NPs in the presence of graphene. Polyvinyl alcohol (PVA), which could be considered as a surface-active agent to help forming homogeneous SnO_2 particles and could effectively transfer to covalent framework at a high temperature, was adopted as a starting carbon material followed by thermal treatment to fabricate a less active carbon substrate to mitigate the volume change during cycling. A small amount of graphene was also included simultaneously to facilitate the transfer of electrons and the transport of electrolyte in the electrode. After hydrothermal treatment with cheap starting materials, *i.e.* polyvinyl alcohol, graphene oxide, stannic chloride and ammonia, carbon-coated SnO_2 NPs were obtained. When used as anode materials in LIBs, the graphene enhanced carbon-coated SnO_2 nanoparticles exhibit a significantly improved cycling performance as compared to carbon-coated SnO_2 NPs without graphene. The result demonstrates that a suitable amount of graphene could effectively improve the cycling performance of the SnO_2-based anode materials in LIBs.

2. Experimental

2.1. Preparation of SnO_2/C composites

In a typical synthesis of the composites, polyvinyl alcohol was gradually added to deionized water (65 mL) along with stirring and then slowly heated to 85 °C for absolute dissolution in a water bath. The above solution is denoted as solution B. Tin(IV) chloride pentahydrate ($SnCl_4 \cdot 5H_2O$) was dissolved in the solution of 60 mL distilled water and 1 mL appropriate concentrated hydrochloric acid under stirring. The obtained solution is labelled as solution C.

Solutions B and C were completely mixed, and their pH values were adjusted to between 9 and 10 by injecting variable amounts of ammonium hydroxide (25.0–38.0 wt%). The above mixture was stirred sufficiently in a water bath for 1 h at 85 °C and then dried at 100 °C for 24 h. Finally, the SnO_2/C composite was obtained after calcination in a tube furnace under high-purity N_2 at 500 °C for 2 h. The as-prepared samples are denoted as SnO_2/C. The contents of SnO_2 in different samples are calculated by the following formula:

$$SnO_2\% = \frac{m_{SnO_2}}{(m_{PVA} + m_{SnO_2})}$$

According to the formula, SnO_2% of SnO_2/C-10, SnO_2/C-30 and SnO_2/C-50 are 10%, 30% and 50%, respectively.

2.2. Preparation of SnO_2/C/GN composites

Graphite oxide was first synthesized from graphite powder by a modified Hummers' method.[32] Graphite oxide (100 mg) was exfoliated in distilled water (100 mL) with ultrasonic treatment (700 W, 1 h) to form a colloidal suspension, and the resultant suspension is marked as solution A. As mentioned above, solutions B and C were prepared and mixed. Solution A was slowly injected into the mixture of solutions B and C. Finally, the SnO_2/C/GN composite was obtained *via* the same process of SnO_2/C. The content of GN in different samples can be approximately estimated by the following equation:

$$GN\% = \frac{m_{GO}}{(m_{PVA} + m_{SnO_2} + m_{GO})}$$

According to the formula, the samples containing 0.7%, 1.5%, 5%, 10% and 15% GN are labelled as SnO_2/C/GN-0.7, SnO_2/C/GN-1.5, SnO_2/C/GN-5, SnO_2/C/GN-10, and SnO_2/C/GN-15, respectively.

For comparison, the control samples of pure SnO_2, C/GN (carbonized PVA with 1.5 wt% graphene) and SnO_2/GN (50 wt% SnO_2 coated by graphene) were synthesized by the same method as mentioned above.

2.3. Sample characterization

The structures and morphologies of the samples were characterized by X-ray diffraction (XRD) (X'Pert PRO MPD, Holland), field emission scanning electron microscopy (FE-SEM) (Hitachi S-4800, Japan), and transmission electron microscopy (TEM) (JEM-2100UHR, Japan). The functional groups in the samples were characterized by Fourier transform infrared spectrometry (FTIR) (Thermo Nicolet NEXUS 670, USA). The thermal properties and the compositions of the samples were characterized by thermogravimetric analysis (TGA) (STA 409 PC Luxx, Germany).

2.4. Electrochemical measurements

The as-prepared samples were mixed with carbon black and poly(vinylidene) fluoride (PVDF) binder (80 : 10 : 10 in weight ratio) in *N*-methyl-2-pyrrolidinone (NMP) to form a homogeneous slurry, which was then coated onto a copper foil current

collector to prepare the working electrode. The prepared working electrode was dried in a vacuum oven at 100 °C for 10 h and then assembled into a half-battery in an Ar-filled glove box. The half-battery (CR2032 coin type) was manufactured by employing the as-prepared materials as the working electrode, Li foil as the counter electrode and the reference electrode, a microporous polypropylene film as the separator, and 1 mol L^{-1} $LiPF_6$ in a 1 : 1 (v/v) mixture of ethylene carbonate (EC) and dimethyl carbonate (DMC) as the electrolyte. The cells were galvanostatically charged–discharged in the potential range of 0.005–2.5 V *vs.* Li/Li^+ at the current densities of 100, 200, 400 and 800 mA g^{-1} on a Land CT2001A cycler. Cyclic voltammograms (CV) were performed using an Ametek PARSTAT4000 electrochemistry workstation at 0.25 mV s^{-1} within the potential range of 0.01–2.5 V.

3. Results and discussion

XRD patterns of SnO_2/C/GN-1.5 and SnO_2/GN are shown in Fig. 1. The peak of GO at 11.4° (see Fig. S1(c)†), which represents the weak van der Waals force between layers of GO, could not be identified in Fig. 1(a) because of the addition of a small amount of GO, the disordered stacking characteristics of the graphene sheets and the disordered nature of carbon.[33,34] The higher angle peak of sample C/GN in Fig. S1(b)† of the *d*3 spacing at 25.5° corresponds to a distance of approximately 3.49 Å that can be assigned to the π–π stacking between aromatic rings. The four dominant broad peaks (110), (101), (211), and (301) are attributed to the SnO_2 phase (JCPDS no. 41-1445), indicating the formation of a tetragonal SnO_2 nanocrystal.

These diffraction peaks in SnO_2/C/GN-1.5 are obviously stronger than those of SnO_2/C-50 (see Fig. S1(a)†), which suggests the higher crystallinity due to the introduction of GO. In all cases, the peak of carbon could not be identified, which reveals the amorphous carbon in the mixture. The XRD pattern of SnO_2/GN in Fig. 1(b) is similar to that of SnO_2/C/GN-1.5. The four dominant broad peaks (110), (101), (211), and (301) are attributed to the SnO_2 phase, which are stronger and broader than those of SnO_2/C/GN-1.5. It indicates that the tetragonal SnO_2 nanocrystals are well formed through the addition of crystalline GN.

As shown in Fig. 2, the FTIR spectrum of carbonized PVA (C-PVA) shows the stretching vibrations of C=C and aromatic cycles around 1580 cm^{-1} and the strong transmission from 900 cm^{-1} to 600 cm^{-1} could be signed as the fingerprint region of C–H on an aromatic cycle.[35,36] The injection of the Sn^{4+} ion into PVA and high temperature treatment introduces a strong peak at 580 cm^{-1}, which is ascribed to Sn–O in the curve of SnO_2/C and the mentioned peaks on C-PVA could also be identified. After the addition of GO in the mixture, as shown in the profiles of SnO_2/C/GN, the thermal treatment eliminates most of the oxygen-containing groups on GO such as COOH peaks (1735 cm^{-1}), C–O stretching vibrations (1052 cm^{-1}), the O–H deformation peak (1401 cm^{-1}) and the O–C=O peak (827 cm^{-1}), which indicates that GO has been reduced to graphene to some degree. The transmission curves of SnO_2/C/GN are almost the same as those of SnO_2/C except a new peak at 640 cm^{-1}, which might come from the aromatic cycles. The introduction of GN seems to play some positive role in aromatization during the thermal carbonization. The FT-IR spectra of graphite oxide and SnO_2 are shown in Fig. S2.†

In order to assess the thermal property and the composition of SnO_2/C/GN-1.5, thermogravimetric analysis (TGA) is employed in air. As shown in Fig. 3, the first major weight loss (about 6%) in the range of 40–150 °C corresponds to the removal of absorbed H_2O. It is revealed that a significant weight loss takes place at 300–600 °C, which should be attributed to the combustion of amorphous carbon and graphene. Finally, only

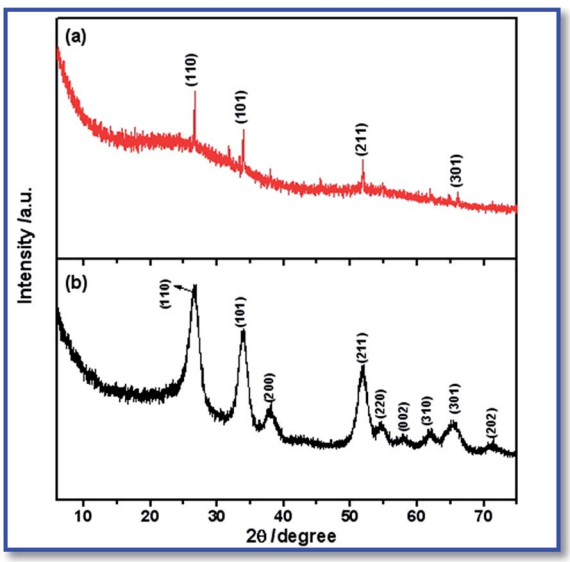

Fig. 1 XRD patterns of (a) SnO_2/C/GN-1.5 and (b) SnO_2/GN.

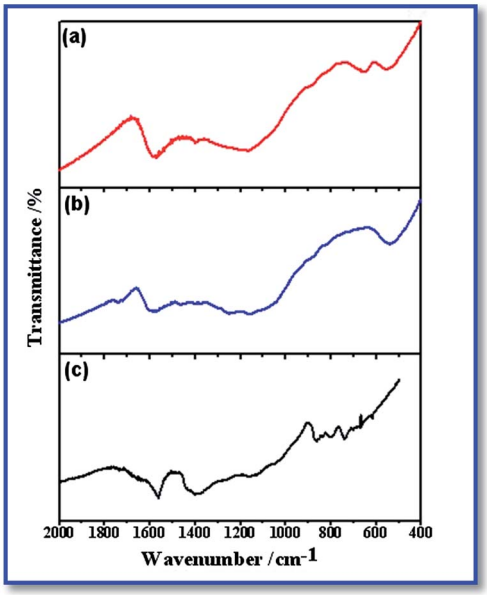

Fig. 2 FT-IR spectra of (a) SnO_2/C/GN-1.5, (b) SnO_2/C-50 and (c) C-PVA.

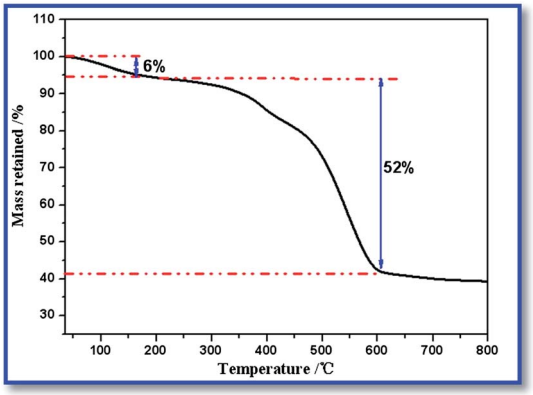

Fig. 3 TGA curve of SnO_2/C/GN-1.5 in air.

SnO_2 NPs were left. Based on the weight loss in the TGA curve, the SnO_2 content in SnO_2/C/GN-1.5 could be estimated, *i.e.* 42%, which is relatively lower than 50% of the calculated value. This variation may originate from the addition of graphene oxide, absorbed water and decomposition of products due to thermal treatment.

The morphologies of SnO_2/C/GN-1.5 and SnO_2/C-50 samples are studied by field emission transmission electronic microscopy (TEM) in Fig. 4. In Fig. 4(a), SnO_2/C/GN-1.5 is formed by bulk carbon particles with SnO_2 NPs homogeneously dispersed inside them (darker dots). In Fig. 4(b), the high-resolution (HR) TEM image of SnO_2/C/GN-1.5 is presented and the lattice fringes of SnO_2 NPs are clearly visible (see inset). The interlayer spacings are about 0.33 nm and 0.26 nm respectively corresponding to (110) and (101) planes of SnO_2. Thin layers of carbon in the form of stacked graphene sheets can be found on the edges of SnO_2 particles (*cf.* arrows). Therefore, the SnO_2 NPs are wrapped between the graphene sheets and the amorphous carbon coating layers, which provides a perfectly conductive carbon network, facilitating electron transfer, buffering the volume changes, preventing the aggregation of SnO_2 NPs, and maintaining the contact between graphene sheets and SnO_2 NPs during Li^+ insertion/extraction, thus improving the electrochemical performance as an anode material for LIBs. SnO_2 NPs also disperse well in SnO_2/C-50 as described in Fig. 4(c) and (d), and some SnO_2 nanocrystals could be identified. It is noted that the sizes of SnO_2 nanocrystals are somewhat larger than those in SnO_2/C/GN-1.5, and most of the SnO_2 particles still exist in the amorphous state, which has been proved in the XRD images. The TEM images of the control sample SnO_2/GN are shown in Fig. S4(a) and (b).† The SnO_2 nanocrystals are distributed uniformly on the surface of GN and the sizes are smaller than those in SnO_2/C/GN-1.5, which have also been confirmed by XRD. The GN conjugated planes seem to have some special interaction with SnO_2, which could help the growth and distribution of SnO_2 nanocrystals. In sample C/GN (see Fig. S4(c)†), crystalline structures could not be identified, which reveals the amorphous carbon in the composite.

Field emission scanning electron microscopy (FE-SEM) images in Fig. S3† show that SnO_2/C-50 and SnO_2/C/GN-1.5 have an almost uniform morphology over large domains. Both SnO_2/C-50 and SnO_2/C/GN-1.5 can be imaged well without Au coating, which suggests that the obtained samples possess good electrical conductivities. The high resolution images give the distribution details of SnO_2 NPs on the surface of amorphous carbon (Fig. S3(a) and (b)†). In all cases, the SnO_2 NPs are distributed on the carbon matrix. SnO_2 NPs in SnO_2/C-50 have a diameter of about 50 nm and a little larger in SnO_2/C/GN-1.5, both of which are covered by a carbon layer.

The involvement of GO seems to not only increase the crystallinity of SnO_2, but also avoids particle agglomeration. Based on the experiment data, we propose a possible mechanism for material manufacturing (Fig. 5). Initially, most of the injected Sn^{4+} ions interact with –OH groups on the PVA chains, which could be considered as a surfactant. When GO with many oxygen-containing groups is added to the above mixture, the formation of interfacial bonds between graphene oxide sheets and PVA molecules interacted with Sn^{4+} ions and these are favourable to the stabilization of SnO_2 NPs decorated on graphene oxide sheets. During the following assembling process, SnO_2 nanocrystals could grow up in higher crystalline size and

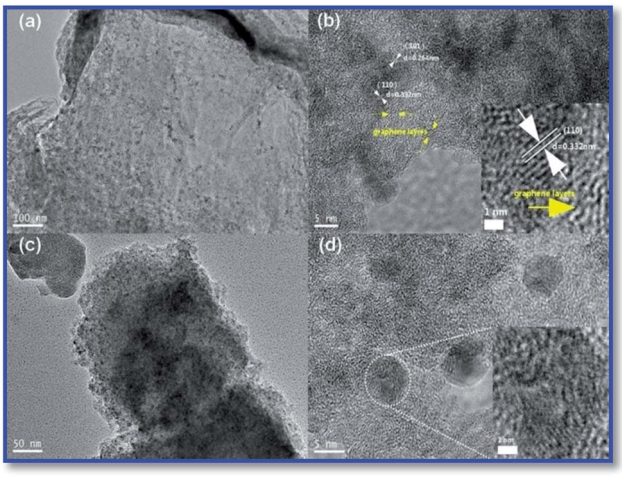

Fig. 4 TEM images of (a) SnO_2/C/GN-1.5 and (c) SnO_2/C-50 and HRTEM images of (b) SnO_2/C/GN-1.5 and (d) SnO_2/C-50.

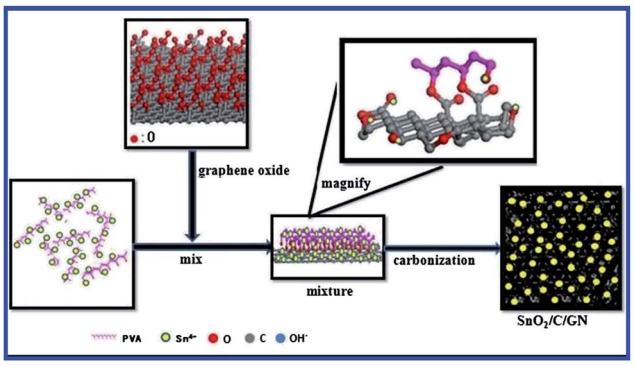

Fig. 5 Schematic of the synthesis and the structure of SnO_2/C/GN.

the voids existing between individual composite sheets could be fixed by carbonized PVA for stabilization. Graphene oxide sheets act as crystal nuclei for promoting the growth and distribution of SnO_2 nanocrystals, which have been confirmed by XRD and TEM.

To evaluate the abilities of SnO_2 based carbon materials in Li^+ storage, the samples are used as the anodes for LIBs. The first cycle for charge–discharge properties of three graphene-free samples (SnO_2/C-10, SnO_2/C-30 and SnO_2/C-50) at a current density of 100 mA g^{-1} and a voltage cut-off of 2.5/0.005 V *versus* Li/Li^+ are shown in Fig. 6. As shown in Fig. 6(a), with increasing amounts of SnO_2, the capacities of the first discharge–charge increased simultaneously, which are 443/427, 984/710 and 1267/924 mA h g^{-1}, respectively. The residual capacity between 20^{th} and 30^{th} circles is clearly shown in Fig. 6(b), the initial capacity losses are about 52%, 57%, and 66% for SnO_2/C-10, SnO_2/C-30 and SnO_2/C-50 after 30 cycles, respectively. Similar to a bulk SnO_2 system, the electrochemical curves of SnO_2/C show an extended plateau around 0.8 V in the first discharge, which is well known as the reaction of SnO_2 with lithium to form the solid electrolyte interface (SEI) layers.[23,37]

As shown in Fig. 6, all the three samples have a large and irreversible capacity, which is due to the formation of the amorphous Li_2O matrix and the intense surface reactions between Li–Sn compounds and the electrolyte solution. It is well known that the rapid fading of the SnO_2 electrode is mainly caused by a large volume expansion of SnO_2 occurring during the charge–discharge cycle, leading to the pulverization of the electrode. The improved electrochemical performance observed in our experiments should be attributed to the synergetic effect of SnO_2 and the carbonaceous material. The carbonaceous material itself could store Li^+ and acts as an electronic conductor. Furthermore, the carbonaceous material in SnO_2 based composites can limit the volume expansion during the process of lithium insertion.

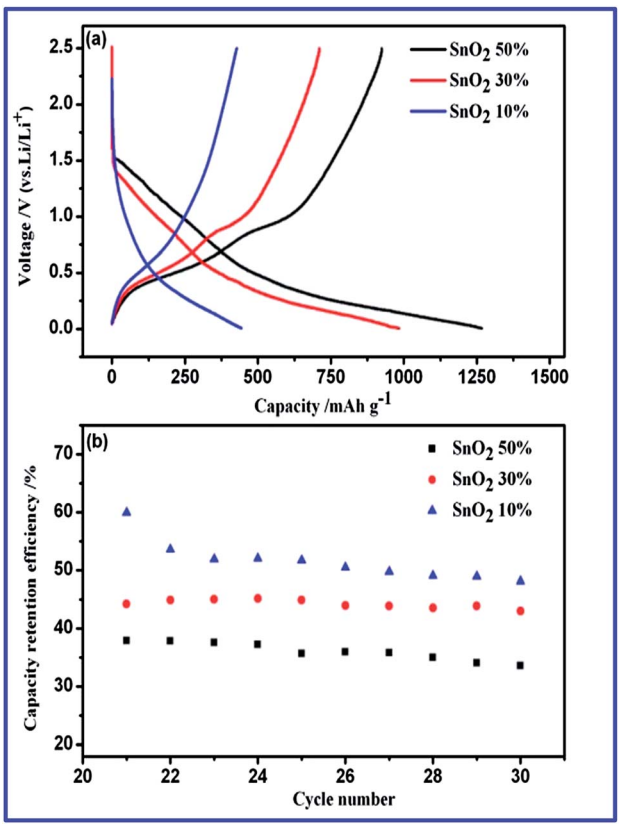

Fig. 6 (a) Charge–discharge profiles and (b) capacity retention efficiency profiles of SnO_2/C-10, SnO_2/C-30 and SnO_2/C-50.

In order to have a larger initial capacity and better retention of the reversible capacity for a long term cycling, SnO_2/C-50 with high initial capacity is used as the starting material and is added to GO before thermal treatment and then carbonized at 500 °C. The resultant samples with varied GO contents are used as the anodes for LIBs.

Fig. 7(a) shows a comparison of the cyclic performances at a current density of 100 mA g^{-1} for SnO_2/C/GN-0.7, SnO_2/C/GN-1.5, SnO_2/C/GN-5, SnO_2/C/GN-10, and SnO_2/C/GN-15. For the 5^{th} cycle, the capacities of all the five samples are over 600 mA h g^{-1} except for SnO_2/C/GO-0.7, which are much better than 565 mA h g^{-1} of SnO_2/C-50. SnO_2/C/GN-1.5 possesses the best cycling stability in all of the five samples, which is still above 720 mA h g^{-1} even after 70 cycles. The capacity retention of SnO_2/C/GN-1.5 after 30 cycles is about 70%, much higher than 34% of SnO_2/C-50 (see Fig. 6(b)). This electrochemical improvement on SnO_2/C/GN is due to the introduction of GN. The high surface area and excellent electrical conductivity of graphene not only provide the channels for electron transfer and the transport of electrolyte in the carbon layer, but also help the formation and dispersion of SnO_2 NPs during carbonization, which has also been confirmed by XRD. A higher content of GN in SnO_2/C/GN does not lead to a better electrochemical performance, which may be explained as follows. The conductivity of SnO_2/C/GN with 1.5 wt% GN is good enough for charge transfer during cycling. Meanwhile, the interactions between GN sheets are not as strong as that between GN and PVA after thermal treatment. So, the higher loading of GN would weaken the mechanical strength and cause the easier pulverization of the electrode during charge–discharge cycles.

In our experiments, SnO_2/C/GN-1.5 exhibits the best electrochemical performances as shown in Fig. 7(b). In the first cycle, SnO_2/C/GN-1.5 delivers a discharge capacity of 1312 mA h g^{-1} and a charge capacity of 1273 mA h g^{-1} at a current density of 100 mA g^{-1}. The Coulombic efficiency of the first cycle is as high as 96%, which is much higher than 72% of SnO_2/C-50. The high Coulombic efficiency of SnO_2/C/GN-1.5 is believed to be mainly due to the introduction of GN.[38] As shown in Fig. 7(c), the discharge capacity of SnO_2/C/GN-1.5 is still up to 720 mA h g^{-1} after 70 cycles. SnO_2 NPs on graphene are found less aggregating into larger clusters, which might contribute to the excellent cycling stability of SnO_2/C/GN-1.5. In order to better understand the reaction mechanism during charge–discharge cycles, cyclic voltammetry of SnO_2/C/GN-1.5 is given in Fig. 7(d). In the first cycle, the weak irreversible cathodic peak around 0.74 V is attributed to the formation of the solid electrolyte interface layer. This peak is not presented

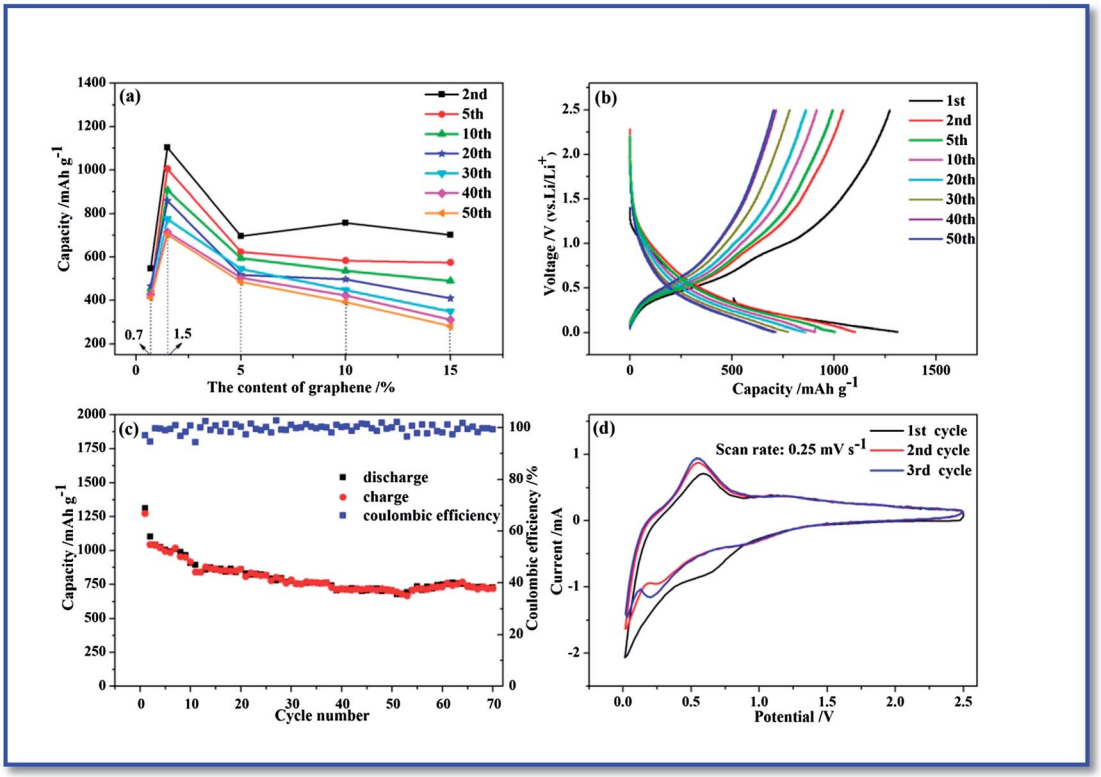

Fig. 7 (a) Specific capacity *vs.* graphene content, (b) the charge–discharge profiles of SnO_2/C/GN-1.5, (c) the cyclic performance of SnO_2/C/GN-1.5 and (d) the cyclic voltammograms of SnO_2/C/GN-1.5.

in the second cycle and afterwards. The clear cathodic peak around 0.22 V and the anodic peak around 0.54 V are related to the lithium alloying reaction with Sn and dealloying of Li_xSn, respectively. The rate performance of SnO_2/C/GN-1.5 evaluated at various current densities is presented in the ESI (Fig. S5(a)†). It is evident that the graphene framework has greatly improved the electron transfer and the stability of the SnO_2/C/GN electrode compared to the pure SnO_2 electrode. At a current density of 400 mA g^{-1}, SnO_2/C/GN-1.5 delivers a high capacity of 560 mA h g^{-1}, and rebounds back to 840 mA h g^{-1} when the current density swings back to 100 mA g^{-1}, which is still much higher than 372 mA h g^{-1} of the theoretical capacity of graphite.

The control experiments are carried out with pure SnO_2, C/GN and SnO_2/GN as the anode materials in LIBs at a current rate of 100 mA g^{-1} under the same experimental conditions as those for SnO_2/C/GN. Fig. S5(b)† shows the cycling performance of pure SnO_2, C/GN and SnO_2/GN, respectively. The capacities of the initial discharge–charge are 1219/599, 332/110 and 1391/704 mA h g^{-1}, respectively. After 35 cycles, the remaining capacities are 290, 81 and 565 mA h g^{-1}, which retain 23.8, 24.4 and 40.6%, respectively. The best electrochemical performance of the above three samples is reported for SnO_2/GN, which is still much lower than that of SnO_2/C/GN-1.5. These data furthermore demonstrate that the C-PVA shell indeed has a great positive effect on the electrochemical stability of SnO_2.

4. Conclusions

A simple and effective protocol was presented to fabricate SnO_2/carbon/graphene nanocomposites with different compositions and nanostructures. PVA is selected as the cheap and readily available carbon source to form the supporting matrix for SnO_2 nanoparticles. The results show that the changes in the ratios of SnO_2 and graphene oxide can control the capacity of SnO_2/carbon/graphene. The improvement in the electrochemical performance of SnO_2/carbon/graphene can be achieved by "doping" a certain amount of graphene. As ascribed to the synergetic effects of a unique combination of material properties, SnO_2/C/GN-1.5 with only 1.5 wt% GN shows a stable capacity at 720 mA h g^{-1} after 70 cycles, which uses much less GN in comparison to those in a previous report. The planar graphene structure in SnO_2/C/GN could not only improve the electrical conductivity, but also increase the crystallinity of SnO_2 and avoid particle agglomeration, which are beneficial for accommodating the large volume expansion and facilitating the electron transfer. The method described in this paper may provide a simple, economic and effective strategy for the preparation of metal-oxide/carbon/graphene composites.

Acknowledgements

This work was supported by the National Natural Science Foundation of China (nos 51303212, 51172285, and 51372277);

the National Natural Science Foundation of Shandong Province (ZR2013EMQ013); the Fundamental Research Fund for the Central Universities (14CX02060A).

Notes and references

1 Y. Idota, T. Kubota, A. Matsufuji, Y. Maekawa and T. Miyasaka, *Science*, 1997, **276**, 1395.
2 T. Nokami, T. Matsuo, Y. Inatomi, N. Hojo, T. Tsukagoshi, H. Yoshizawa, A. Shimizu, H. Kuramoto, K. Komae, H. Tsuyama and J. Yoshida, *J. Am. Chem. Soc.*, 2012, **134**, 19694.
3 B. Luo, B. Wang, M. H. Liang, J. Ning, X. L. Li and L. J. Zhi, *Adv. Mater.*, 2012, **24**, 1405.
4 J. R. Dahn, T. Zheng, Y. Liu and J. S. Xue, *Science*, 1995, **270**, 590.
5 A. Magasinski, P. Dixon, B. Hertzberg, A. Kvit, J. Ayala and G. Yushin, *Nat. Mater.*, 2010, **9**, 353.
6 A. M. Chockla, K. C. Klavetter, C. B. Mullins and B. A. Korgel, *Chem. Mater.*, 2012, **24**, 3738.
7 I. Kovalenko, B. Zdyrko, A. Magasinski, B. Hertzberg, Z. Milicev, R. Burtovyy, I. Luzinov and G. Yushin, *Science*, 2011, **333**, 75.
8 Y. L. Wang, T. Y. Wang, P. M. Da, M. Xu, H. Wu and G. F. Zheng, *Adv. Mater.*, 2013, **25**, 5177.
9 W. M. Zhang, J. S. Hu, Y. G. Guo, S. F. Zheng, L. S. Zhong, W. G. Song and L. J. Wan, *Adv. Mater.*, 2008, **20**, 1160.
10 R. Yang, Y. Gu, Y. Li, J. Zheng and X. Li, *Acta Mater.*, 2010, **58**, 866.
11 M. Winter and J. O. Besenhard, *Electrochim. Acta*, 1999, **45**, 31.
12 Y. Wang, J. Y. Lee and H. C. Zeng, *Chem. Mater.*, 2005, **17**, 3899.
13 M. S. Park, Y. M. Kang, G. X. Wang, S. X. Dou and H. K. Liu, *Adv. Funct. Mater.*, 2008, **18**, 455.
14 C. F. Zhang, X. Peng, Z. P. Guo, C. B. Cai, Z. X. Chen, D. Wexler, S. Li and H. K. Liu, *Carbon*, 2012, **50**, 1897.
15 J. W. Zhu, S. Chen, X. D. Wu, Q. F. Han and X. Wang, *ACS Nano*, 2010, **4**, 2822.
16 R. S. Ruoff, Y. W. Zhu, S. Murali, M. D. Stoller, K. J. Ganesh, W. W. Cai, P. J. Ferreira, A. Pirkle, R. M. Wallace, K. A. Cychosz, M. Thommes, D. Su and E. A. Stach, *Science*, 2011, **332**, 1537.
17 M. S. Park, Y. M. Kang, J. H. Kim, G. X. Wang, S. X. Dou and H. K. Liu, *Carbon*, 2008, **46**, 35.
18 R. Yang, W. Zhao, J. Zheng, X. Z. Zhang and X. G. Li, *J. Phys. Chem. C*, 2010, **114**, 20272.
19 Y. S. Jung, K. T. Lee and S. M. Oh, *Electrochim. Acta*, 2007, **52**, 7061.
20 X. W. Lou, C. M. Li and L. A. Archer, *Adv. Mater.*, 2009, **21**, 2536.
21 L. J. Fu, H. Liu, H. P. Zhang, C. Li, T. Zhang, Y. P. Wu, R. Holze and H. Q. Wu, *Electrochem. Commun.*, 2006, **8**, 1.
22 X. He, W. Pu, L. Wang, J. Ren, C. Jiang and C. Wan, *Solid State Ionics*, 2007, **178**, 833.
23 S. M. Paek, E. J. Yoo and I. Honma, *Nano Lett.*, 2009, **9**, 72.
24 J. Yao, X. P. Shen, B. Wang, H. K. Liu and G. X. Wang, *Electrochem. Commun.*, 2009, **11**, 1849.
25 D. Larcher, S. Beattie, M. Morcrette, K. Edstroem, J. C. Jumas and J. M. Tarascon, *J. Mater. Chem.*, 2007, **17**, 3759.
26 H. W. Song, N. Li, H. Cui and C. X. Wang, *J. Mater. Chem. A*, 2013, **1**, 7558.
27 X. S. Zhou, Y. X. Yin, L. J. Wan and Y. G. Guo, *J. Mater. Chem.*, 2012, **22**, 17456.
28 G. Ji, B. Ding, Z. Sha, J. S. Wu, Y. Ma and J. Y. Lee, *Nanoscale*, 2013, **5**, 5965.
29 R. L. Liang, H. Q. Cao, D. Qian, J. X. Zhang and M. Z. Qu, *J. Mater. Chem.*, 2011, **21**, 17654.
30 B. J. Li, H. Q. Cao, J. X. Zhang, M. Z. Qu, F. Lian and X. H. Kong, *J. Mater. Chem.*, 2012, **22**, 2851.
31 C. F. Zhang, X. Peng, Z. P. Guo, C. B. Cai, Z. X. Chen, D. Wexler, S. Li and H. K. Liu, *Carbon*, 2012, **50**, 1897.
32 W. S. Hummers and R. E. Offeman, *J. Am. Chem. Soc.*, 1958, **80**, 1339.
33 Y. X. Xu, K. X. Sheng, C. Li and G. Q. Shi, *ACS Nano*, 2010, **4**, 4324.
34 M. Zhang, D. N. Lei, Z. F. Du, X. M. Yin, L. B. Chen, Q. H. Li, Y. G. Wang and T. H. Wang, *J. Mater. Chem.*, 2011, **21**, 1673.
35 R. Bissessur, P. K. Y. Liu, W. White and S. F. Scully, *Langmuir*, 2006, **22**, 1729.
36 J. Peckett, P. Trens, R. Gougeon, A. Poppl and R. Harris, *Carbon*, 2000, **38**, 345.
37 X. Sun, J. Liu and Y. Li, *Chem. Mater.*, 2006, **18**, 3486.
38 Q. Guo, Z. Zheng, H. L. Gao, J. Ma and X. Qin, *J. Power Sources*, 2013, **240**, 149.